J. Marine Sci. Appl. (2015) 14: 343-354
DOI: 10.1007/s11804-015-1329-3

Path-tracking Control of Underactuated Ships Under Tracking Error Constraints

Khac Duc Do*

Department of Mechanical Engineering, Curtin University, Kent Street, Bentley, WA 6102, Australia

Abstract: This paper presents a constructive design of new controllers that force underactuated ships under constant or slow time-varying sea loads to asymptotically track a parameterized reference path, that guarantees the distance from the ship to the reference path always be within a specified value. The control design is based on a global exponential disturbance observer, a transformation of the ship dynamics to an almost spherical form, an interpretation of the tracking errors in an earth-fixed frame, an introduction of dynamic variables to compensate for relaxation of the reference path generation, *p*-times differentiable step functions, and backstepping and Lyapunov's direct methods. The effectiveness of the proposed results is illustrated through simulations.
Keywords: underactuated ship; path-tracking; error constraint; Lyapunov method; backstepping method

Article ID: 1671-9433(2015)04-0343-12

1 Introduction

The main difficulty with controlling an underactuated ship is that only the yaw and surge axes are directly actuated while the sway axis is not. An application of Brockett's theorem (Brockett, 1983) shows nonexistence of pure-state feedbacks that are able to asymptotically stabilize an underactuated ship at a fixed point. Thus, the stabilization problem is often solved by either discontinuous or time-varying feedback (e.g., (Reyhanoglu, 1997; Pettersen and Egeland, 1996; Aguiar and Pascoal, 2001; Mazenc *et al*., 2002; Do *et al*., 2002b)).

A global exponential position tracking system without controlling the ship's yaw angle was proposed in (Godhavn *et al*., 1998). In (Pettersen and Nijmeijer, 2001), a high-gain, local exponential tracking result was obtained based on the work in (Jiang and Nijmeijer, 1999). Based on cascade and passivity approaches, several global tracking results were obtained in (Lefeber *et al*., 2003; Jiang, 2002). Note that in (Jiang, 2002; Lefeber *et al*., 2003; Pettersen and Nijmeijer, 2001), the yaw velocity was required to be nonzero, i.e., a straight-line cannot be tracked. This restrictive assumption was removed in (Do *et al*., 2002a; 2002b; Lee and Jiang, 2004), where various relaxations on the reference trajectory and ship dynamics were made, see also (Chwa, 2011) for a solution to the tracking problem with input constraints. An assumption of low speed (nonlinear damping terms are ignored) is usually made in the above works due to the complex generation of the reference trajectories, and difficulties in stability analysis (especially stability analysis of the sway dynamics).

There are three main approaches to path-following control of ships. In the first approach, the Serret-Frenet frame is used to define the path-following (cross-track and yaw angle) errors, then the yaw moment control input is designed to stabilize these errors at the origin (e.g., (Skjetne and Fossen, 2001; Encarnação *et al*., 2000; Do and Pan, 2004; Li *et al*., 2009) for nonlinear (curved) paths, (Pettersen and Lefeber, 2001; Fredriksen and Pettersen, 2006; Moreira *et al*., 2007) for linear (straight) paths). This approach results in local results (except for the linear path) due to singularity in the cross-track error dynamics. The second approach defines the path-following objective as one of controlling the vessel so that it is in the tube of nonzero diameter centered on the path, and moves along the path with a desired speed (e.g., (Aicardi *et al*., 2001; Do *et al*., 2004; Li *et al*., 2008)). The control design aims to force the vessel to follow a virtual point moving along the path. This approach requires the vessel not be too close to the path. The third approach (referred to as path-tracking) is based on a combination of trajectory-tracking and path-following in the first approach. In the sense that the lateral path-following error is not always set to zero (to avoid singularity) and that the path parameter is used as an additional control to stabilize the lateral path-following error. Thus, global control results are often obtained (e.g., (Lapierre and Jouvencel, 2008; Do and Pan, 2006; Ghommam *et al*., 2008)).

In all of the above works on trajectory-tracking and path-following control of underactuated ships, a hard constraint on the tracking/following errors has never been addressed. This problem is important since in practice it is desired to steer the ship to be within a certain distance from the reference path, especially in narrow waterways. Moreover, various conditions on the control gains and reference paths/trajectories were imposed in the existing mentioned works to ensure boundedness of the sway velocity instead of being directly controlled in the previous control designs. The above issues motivate contributions in this paper on new controllers for asymptotic path-tracking of

Received date: 2015-03-27.
Accepted date: 2015-07-17.
Foundation item: Supported in Part by the Australian Research Council Under Grant No. DP0988424.
***Corresponding author Email:** duc@curtin.edu.au

underactuated ships under constant or slow time-varying sea loads, and a hard constraint on position tracking errors. The method does not require the reference path be generated by a virtual ship. The sway velocity is directly controlled during the control design. First, a disturbance observer is proposed to globally exponentially estimate the sea loads. Second, a primary control surge force is designed to transform the ship dynamics to those of an almost spherical ship. Third, the trajectory tracking errors are represented in the earth-fixed frame and are stabilized at the origin by a design of controllers based on backstepping and Lyapunov's direct methods. A dynamical variable is introduced to the reference yaw angle during the control design to compensate relaxation of the reference path generation.

2 Problem statement

2.1 Equations of motion

Assume that the ship has an *xz*-plane of symmetry; heave, pitch and roll modes are neglected; the body-fixed frame coordinate origin is set in the center-line of the ship. Then, the mathematical model of an underactuated ship moving in a horizontal plane can be described as (Fossen, 2011):

$$\begin{aligned}\dot{\boldsymbol{\eta}} &= \boldsymbol{J}(\psi)\boldsymbol{v}\\ \dot{\boldsymbol{v}} &= \boldsymbol{f}(\boldsymbol{v}) + \boldsymbol{M}^{-1}\tau + \boldsymbol{M}^{-1}\boldsymbol{J}^{-1}(\psi)\theta\end{aligned} \tag{1}$$

where $\eta = \mathrm{col}(x, y, \psi)$ with (x, y) being the (surge, sway) displacements of the center of mass, and ψ being the yaw angle of the ship coordinated in the earth-fixed frame $O_E X_E Y_E$, see Fig. 1; $\boldsymbol{v} = \mathrm{col}(u, v, r)$ denotes the surge, sway, and yaw velocities of the ship coordinated in the body-fixed frame $O_b X_b Y_b$; $\theta = \mathrm{col}(\theta_1, \theta_2, \theta_3)$ denotes the sea loads on the ship along the surge, sway, and yaw axes coordinated in the earth-fixed frame; $\tau = \mathrm{col}(\tau_u, 0, \tau_r)$ denotes the control inputs: the surge force τ_u and yaw moment τ_r; and

$$\boldsymbol{J}(\psi) = \begin{bmatrix}\cos(\psi) & -\sin(\psi) & 0\\ \sin(\psi) & \cos(\psi) & 0\\ 0 & 0 & 1\end{bmatrix},\ \boldsymbol{M} = \begin{bmatrix}m_{11} & 0 & 0\\ 0 & m_{22} & 0\\ 0 & 0 & m_{33}\end{bmatrix}$$

$$\boldsymbol{f}(\boldsymbol{v}) = \left[\frac{m_{22}}{m_{11}}vr - f_1(u), -\frac{m_{11}}{m_{22}}ur - f_2(v), \frac{m_{11}-m_{22}}{m_{33}}uv - f_3(r)\right]^{\mathrm{T}} \tag{2}$$

In (2), (m_{11}, m_{22}) denote the masses including added masses in the surge and sway axes; m_{33} is the inertia including added inertia in the yaw axis; the damping functions $f_1(u)$, $f_2(v)$ and $f_3(r)$ are

$$\begin{aligned}f_1(u) &= \frac{d_{u1}u}{m_{11}} + f_1^{\diamond}(u)u,\ f_2(v) = \frac{d_{v1}v}{m_{22}} + f_2^{\diamond}(v)v\\ f_3(r) &= \frac{d_{r1}r}{m_{33}} + f_3^{\diamond}(r)r\end{aligned} \tag{3}$$

with

$$\begin{aligned}f_1^{\diamond}(u) &= \frac{1}{m_{11}}\sum_{i=2}^{n}\left(d_{u,2i-2}u^{2i-3}\tanh\left(\frac{u}{\varepsilon_0}\right) + d_{u,2i-1}u^{2i-2}\right)\\ f_2^{\diamond}(v) &= \frac{1}{m_{22}}\sum_{i=2}^{n}\left(d_{v,2i-2}v^{2i-3}\tanh\left(\frac{v}{\varepsilon_0}\right) + d_{v,2i-1}v^{2i-2}\right)\\ f_3^{\diamond}(r) &= \frac{1}{m_{33}}\sum_{i=2}^{n}\left(d_{r,2i-2}r^{2i-3}\tanh\left(\frac{r}{\varepsilon_0}\right) + d_{r,2i-1}r^{2i-2}\right)\end{aligned} \tag{4}$$

where n is an integer larger than 1, d_{ui}, d_{vi} and d_{ri} with $i = 1, 2, \ldots$ denote the damping coefficients in the surge, sway, and yaw axes, we use $\bullet\tanh(\bullet/\varepsilon_0)$ with ε_0 being a small positive constant to smoothly approximate $|\bullet|$.

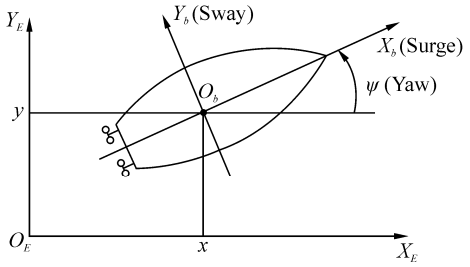

Fig. 1 Definition of coordinate systems and motion variables

Remark 2.1 The mathematical model (1) holds for underactuated ships equipped with two main aft propellers or water jets because the control moment τ_r does not directly enter the sway dynamics. For ships equipped with a rudder, the control force τ_r does directly enter the sway dynamics. Moreover, the off-diagonal terms in the matrix $\boldsymbol{M}$ and the coupling terms in the damping functions $f_1(u)$, $f_2(v)$, and $f_3(r)$ are neglected because these terms are relatively small in comparison with (m_{11}, m_{22}, m_{33}), and those terms already included in $(f_1(u), f_2(v), f_3(r))$, respectively. In the case of ships equipped with a rudder and off-diagonal terms not negligible, the coordinate transformations proposed in (Do and Pan, 2005) and (Do, 2010b) obtain a mathematical model similar to (1). Basically, these coordinate transformations ensure that displacements of a point referred to as the ship's center of oscillation (similar to the case treated in control of aircraft in (Martin *et al*., 1996) and (Do *et al*., 2003)) are controlled instead of displacements of the center of mass of the ship.

2.2 Control objective

In this paper, we study a path-tracking control objective under the following assumptions.

Assumption 2.1

1) The reference path $G(s) = \mathrm{col}(x_d(s), y_d(s))$ with s being the path parameter is four-times differentiable with respect to s and satisfies

$$x_{d'}^2(s) + y_{d'}^2(s) > 0,\quad \forall s \in \mathbb{R} \tag{5}$$

where $x_{d'}(s)=\frac{\partial x_d}{\partial s}$ and $y_{d'}(s)=\frac{\partial y_d}{\partial s}$.

2) The loads θ_1, θ_2 and θ_3 are constant or slow time-varying in the sense that their derivatives with respect to time are negligible and are bounded, i.e., there exist $\theta_i^{\min}$ and $\theta_i^{\max}$ with $i=1,2,3$ such that $\theta_i\in[\theta_i^{\min},\theta_i^{\max}]$.

3) At the initial time $t_0\geq 0$, the position tracking errors $\boldsymbol{q}_e(t_0)=\mathrm{col}(x(t_0)-x_d(s(t_0)),y(t_0)-y_d(s(t_0)))$ satisfy the following condition

$$\|\boldsymbol{q}_e(t_0)\|_N^2<\mu \tag{6}$$

where $\|\boldsymbol{q}_e(t_0)\|_N$ denotes the $\boldsymbol{N}$ weighted norm of $\boldsymbol{q}_e(t_0)$, i.e., $\|\boldsymbol{q}_e(t_0)\|_N^2=\boldsymbol{q}_e^T(t_0)\boldsymbol{N}\boldsymbol{q}_e(t_0)$ with N being a diagonal nonnegative definite matrix, and μ is a positive constant.

Remark 2.2

1) Item 1) of Assumption 2.1 implies that the reference path is sufficiently regular. If the reference path contains several singular points, then we can split it into several nonsingular reference paths and consider each of them separately.

2) Item 2) is reasonable in practice because the actuation systems should not react to high frequency disturbances so as to avoid becoming extensively worn. and we can take sufficiently small bounds $\theta_i^{\min}$ and sufficiently large bounds $\theta_i^{\max}$, $i=1,2,3$.

3) Item 3) means that the position of the ship is within the constrained distance from the reference path at the initial time t_0. Indeed, if the control problem of forcing the ship to asymptotically track the reference path without a distance constraint from the reference trajectory is of interest, one can set $\boldsymbol{N}$ equal to zero. Moreover, if we are only interested in tracking constraint either along the O_EX_E-axis or O_EY_E-axis, the matrix $\boldsymbol{N}$ can be set equal to $\mathrm{diag}(N_1,0)$ or $\mathrm{diag}(0,N_2)$ with N_1 and N_2 being positive constants.

Control Objective 2.1 Design the control inputs τ_u and τ_r, and estimate laws for the loads θ_1, θ_2 and θ_3 so that the following objectives are achieved:

1) The position tracking errors $\boldsymbol{q}_e(t)=\mathrm{col}(x(t)-x_d(s(t)),y(t)-y_d(s(t)))$ are always within the constrained distance from the reference path, i.e.,

$$\|\boldsymbol{q}_e(t)\|_N^2<\mu \tag{7}$$

2) The ship asymptotically tracks the reference path $G(s)$ in the sense that the ship is on the path, and moves forward along the path tangentially with a desired total linear velocity $\vartheta_d(t)$ coordinated in the earth-fixed frame. The velocity $\vartheta_d(t)$ is supposed to be sufficiently regular and sufficiently large to handle sea loads θ_1 and θ_2.

3 Preliminaries

3.1 Smooth saturation function

Definition 3.1 The function $\sigma(x)$ is said to be a smooth saturation function if it is smooth and possesses the properties:

1) $\sigma(x)=0$, if $x=0$, $\sigma(x)x>0$ if $x\neq 0$.

2) $\sigma(-x)=-\sigma(x)$ and $(x-y)[\sigma(x)-\sigma(y)]\geq 0$.

3) $|\sigma(x)|\leq 1$, $|\frac{\sigma(x)}{x}|\leq 1$, and $0<\frac{\mathrm{d}\sigma(x)}{\mathrm{d}x}<1$, for all $(x,y)\in\mathbb{R}^2$.

For the vector $\boldsymbol{x}=\mathrm{col}(x_1,...,x_n)$, the notation $\sigma(\boldsymbol{x})=\mathrm{col}(\sigma(x_1),...,\sigma(x_n))$ is used to denote the smooth saturation function vector of the vector $\boldsymbol{x}$.

3.2 p-times differentiable step function

Definition 3.2 A scalar function $h(x,a,b)$ is said to be a p-times differentiable step function if it enjoys the following properties: 1) $h(x,a,b)=0\,\forall x\in(-\infty,a]$, 2) $h(x,a,b)=1\,\forall x\in[b,\infty)$, 3) $0<h(x,a,b)<1\,\forall x\in(a,b)$, 4) $h(x,a,b)$ is p-times differentiable with respect to x, and 5) $h'(x,a,b)>0\,\forall x\in(a,b)$, where p is a positive integer, $x\in\mathbb{R}$, a and b are constants such that $a<0<b$, $h'(x,a,b)=\frac{\partial h(x,a,b)}{\partial x}$. Moreover, if the function $h(x,a,b)$ is infinite times differentiable with respect to x, then it is said to be a smooth step function.

The following lemma gives a method to construct a p-times differentiable step function.

Lemma 3.1 Let the scalar function $h(x,a,b)$ be defined as

$$h(x,a,b)=\frac{\int_a^x f(\tau-a)f(b-\tau)\mathrm{d}\tau}{\int_a^b f(\tau-a)f(b-\tau)\mathrm{d}\tau} \tag{8}$$

with a and b being constants such that $a<0<b$, and the function $f(y)$ being defined as follows:

$$f(y)=0 \text{ if } y\leq 0,\quad f(y)=g(y) \text{ if } y>0 \tag{9}$$

where $g(y)$ is a single-valued function that enjoys the properties: a) $g(\tau-a)g(b-\tau)>0\quad\forall\tau\in(a,b)$, and b) $g(y)$ is p times differentiable with respect to y and $\lim_{y\to 0^+}\frac{\partial^k g(y)}{\partial y^k}=0, k=1,2,...,p-1,$ with p being a positive integer.

Then the function $h(x,a,b)$ is a p-times differentiable step function. Moreover, if $g(y)$ in (9) is replaced by $g(y)=\mathrm{e}^{-1/y}$ then property 4) is replaced by 4'), i.e., $h(x,a,b)$ is a smooth step function.

Proof. See (Do, 2010a).

4 Exponential disturbance observer

For use in the next section, we here present an observer that globally exponentially estimates the loads θ_1, θ_2, and θ_3.

Lemma 4.1 Let $\hat{\theta}=\mathrm{col}\left(\hat{\theta}_1,\hat{\theta}_2,\hat{\theta}_3,\right)$ be an estimate of θ given by

$$\begin{aligned}&\hat{\theta}=\xi+\boldsymbol{K}_0\boldsymbol{J}(\psi)\boldsymbol{M}\boldsymbol{v}\\&\dot{\xi}=-\boldsymbol{K}_0\boldsymbol{J}(\psi)\boldsymbol{M}(\boldsymbol{f}(\boldsymbol{v})+\boldsymbol{M}^{-1}\tau)-\boldsymbol{K}_0\hat{\theta}-\boldsymbol{K}_0\frac{\partial\boldsymbol{J}(\psi)}{\partial\psi}r\boldsymbol{M}\boldsymbol{v}\\&\xi(t_0)=-\boldsymbol{K}_0\boldsymbol{J}(\psi(t_0))\boldsymbol{M}\boldsymbol{v}(t_0)\end{aligned}\tag{10}$$

where $\boldsymbol{K}_0=\mathrm{diag}(k_{01},k_{02},k_{03})$ with k_{0i}, $i=1,2,3$ being positive constants, and $t_0\geq 0$ is the initial time. Then $\hat{\theta}(t)$ possesses the following properties

$$\hat{\theta}_i(t)=\theta_i\left(1-\mathrm{e}^{-k_{0i}(t-t_0)}\right),\ \hat{\theta}_i(t)\in\left[\theta_i^{\min},\theta_i^{\max}\right]\tag{11}$$

Proof. Let us define $\tilde{\theta}=\theta-\hat{\theta}$, whose derivative along the solutions of (10) and (1) satisfies

$$\dot{\tilde{\theta}}=-\boldsymbol{K}_0\tilde{\theta}\Rightarrow\dot{\tilde{\theta}}_i=-k_{0i}\tilde{\theta}_i\tag{12}$$

for $i=1,2,3,$ because $\boldsymbol{K}_0=\mathrm{diag}(k_{01},k_{02},k_{03})$. Thus, $\tilde{\theta}_i(t)=\tilde{\theta}_i(t_0)\mathrm{e}^{-k_{0i}(t-t_0)}$. This in turn yields (11) since $\hat{\theta}_i(t_0)=0$ by the last equation of (10) and $\theta_i\in[\theta_i^{\min},\theta_i^{\max}]$.

5 Transformation of ship dynamics to an almost spherical form

As discussed in Section 1, we transform the ship dynamics (1) to an almost spherical form by applying the following primary surge force feedback

$$\begin{aligned}\tau_u=&m_{11}\left(\frac{m_{11}}{m_{22}}-\frac{m_{22}}{m_{11}}\right)vr-m_{11}\left(\frac{d_{v1}}{m_{22}}-\frac{d_{u1}}{m_{11}}\right)u-\\&m_{11}(f_2^{\diamond}(v)-f_1^{\diamond}(u))u+m_{11}\tau_u^{\diamond}+\\&(\frac{1}{m_{22}}-\frac{1}{m_{11}})(\cos(\psi)\hat{\theta}_1+\sin(\psi)\hat{\theta}_2)\end{aligned}\tag{13}$$

where $\tau_u^{\diamond}$ is the new control force to be designed. Substituting (13) into (1) results in

$$\begin{aligned}&\dot{\boldsymbol{q}}=\boldsymbol{p}\\&\dot{\boldsymbol{p}}=\boldsymbol{C}_l((\varepsilon-1)r)\boldsymbol{p}-(d_{v1}^{\diamond}+f_2^{\diamond}(v))\boldsymbol{p}+\boldsymbol{J}_l(\psi)\begin{bmatrix}\tau_u^{\diamond}\\0\end{bmatrix}+\\&\quad\frac{1}{m_{22}}\begin{bmatrix}\hat{\theta}_1\\\hat{\theta}_2\end{bmatrix}+\boldsymbol{J}_l(\psi)\boldsymbol{M}_l^{-1}\boldsymbol{J}_l^{-1}(\psi)\begin{bmatrix}\tilde{\theta}_1\\\tilde{\theta}_2\end{bmatrix}\\&\dot{\psi}=r\\&\dot{r}=\frac{m_{11}-m_{22}}{m_{33}}uv-f_3(r)+\frac{1}{m_{33}}\tau_r+\frac{1}{m_{33}}\theta_3\end{aligned}\tag{14}$$

where

$$\begin{aligned}&\boldsymbol{q}=\mathrm{col}(x,y),\ \ \boldsymbol{p}=\boldsymbol{J}_l(\psi)\mathrm{col}(u,v)\\&\boldsymbol{J}_l(\psi)=\begin{bmatrix}\cos(\psi)&-\sin(\psi)\\\sin(\psi)&\cos(\psi)\end{bmatrix}\\&\boldsymbol{C}_l((\varepsilon-1)r)=\begin{bmatrix}0&1\\-1&0\end{bmatrix}(\varepsilon-1)r\\&\boldsymbol{M}_l=\mathrm{diag}(m_{11},m_{22}),\ d_{v1}^{\diamond}=d_{v1}/m_{22},\varepsilon=m_{11}/m_{22}\end{aligned}\tag{15}$$

It is noted that $\varepsilon<1$ because the added mass in the sway axis is always larger than that in the surge axis for surface ships.

6 Control design

A close look at the system (14) shows that it consists of two subsystems: the linear motion subsystem $(\boldsymbol{q},\boldsymbol{p})$ and the rotational motion subsystem (ψ,r). These two subsystems are connected via the terms $\boldsymbol{C}_l((\varepsilon-1)r)\boldsymbol{p}$ and $\boldsymbol{J}_l(\psi)\mathrm{col}(\tau_u^{\diamond},0)$. The term $\boldsymbol{C}_l((\varepsilon-1)r)\boldsymbol{p}$ causes a problem in applying the backstepping method in Krstić *et al*. (1995) because $\dot{\psi}=r$. Thus, care needs to be taken to resolve this problem, see 6.1. The control design consists of three steps. In the first step, $\tau_u^{\diamond}$ and ψ will be considered as controls to force the position vector $\boldsymbol{q}$ to track its reference trajectory $\boldsymbol{q}_d=\mathrm{col}(x_d,y_d)$, and to guarantee the tracking errors are within the constraint. In the second step, the yaw velocity r will be treated as a virtual control to stabilize the error between the yaw angle and its virtual value at the origin. The control τ_r will be designed in the last step to stabilize the error between the yaw velocity r and its virtual value at the origin.

6.1 Step 1

Let us define

$$\begin{cases}\psi_d=\arctan(\dfrac{y_{d'}}{x_{d'}})\\ \vartheta_d=\sqrt{x_{d'}^2+y_{d'}^2}\,\dot{s}\end{cases},\ \boldsymbol{q}_d=\begin{bmatrix}x_d\\y_d\end{bmatrix},\ \boldsymbol{p}_d=\begin{bmatrix}\dot{x}_d\\\dot{y}_d\end{bmatrix}\tag{16}$$

It now can be seen that the reference path $\boldsymbol{q}_d$ is generated by the following dynamical system

$$\dot{\boldsymbol{q}}_d = \boldsymbol{p}_d$$
$$\dot{\boldsymbol{p}}_d = \dot{\vartheta}_d \begin{bmatrix} \cos(\psi_d) \\ \sin(\psi_d) \end{bmatrix} + \dot{\psi}_d \begin{bmatrix} -\dot{y}_d \\ \dot{x}_d \end{bmatrix} \tag{17}$$

We define the tracking errors

$$\boldsymbol{q}_e = \boldsymbol{q} - \boldsymbol{q}_d, \quad \boldsymbol{p}_e = \boldsymbol{p} - \boldsymbol{p}_d \tag{18}$$

Differentiating both sides of (18) along the solutions of (17) and the first two equations of (14) gives

$$\begin{aligned} &\dot{\boldsymbol{q}}_e = \boldsymbol{p}_e \\ &\dot{\boldsymbol{p}}_e = \boldsymbol{C}_l((\varepsilon-1)r)\boldsymbol{p}_e - (d_{v1}^{\diamond} + f_2^{\diamond}(v))\boldsymbol{p}_e + \boldsymbol{C}_l((\varepsilon-1)r)\boldsymbol{p}_d + \\ &\quad \boldsymbol{J}_l(\psi)\begin{bmatrix} \tau_u^{\diamond} \\ 0 \end{bmatrix} + \frac{1}{m_{22}}\begin{bmatrix} \hat{\theta}_1 \\ \hat{\theta}_2 \end{bmatrix} + \boldsymbol{J}_l(\psi)\boldsymbol{M}_l^{-1}\boldsymbol{J}_l^{-1}(\psi)\begin{bmatrix} \tilde{\theta}_1 \\ \tilde{\theta}_2 \end{bmatrix} - \\ &\quad (d_{v1}^{\diamond} + f_2^{\diamond}(v))\boldsymbol{p}_d - \dot{\vartheta}_d \begin{bmatrix} \cos(\psi_d) \\ \sin(\psi_d) \end{bmatrix} - \dot{\psi}_d \begin{bmatrix} -\dot{y}_d \\ \dot{x}_d \end{bmatrix} \end{aligned} \tag{19}$$

We define

$$\psi_e = \psi - \alpha_\psi \tag{20}$$

where α_ψ is a virtual control of ψ, and consider the following Lyapunov function candidate

$$V_1 = \gamma + \beta \tag{21}$$

The function γ is designed such that it penalizes the position tracking errors between the reference and actual trajectories of the ship. This function is chosen as follows:

$$\gamma = \int_0^{q_e} \sigma^{\mathrm{T}}(\chi)\boldsymbol{K}_1 \mathrm{d}\chi + \frac{1}{2}\| \boldsymbol{p}_e \|^2 \tag{22}$$

where $\sigma(\bullet)$ is the smooth saturation function vector of the vector $\bullet$ defined in Subsection 3.1, $\boldsymbol{K}_1 = \mathrm{diag}(k_{11}, k_{12})$ with k_{11} and k_{12} being positive constants. The function β needs to be nonnegative definite when the ship is within the constrained distance from the reference path, be equal to zero when the position tracking errors are equal to zero, and be equal to infinity when the ship reaches the constrained distance from the reference path. We propose the function β as follows

$$\beta = \frac{h(\boldsymbol{q}_e^{\mathrm{T}}\boldsymbol{N}\boldsymbol{q}_e, a, b)\boldsymbol{q}_e^{\mathrm{T}}\boldsymbol{N}\boldsymbol{q}_e}{[\mu - h(\boldsymbol{q}_e^{\mathrm{T}}\boldsymbol{N}\boldsymbol{q}_e, a, b)\boldsymbol{q}_e^{\mathrm{T}}\boldsymbol{N}\boldsymbol{q}_e]^2} \tag{23}$$

where $h(\boldsymbol{q}_e^{\mathrm{T}}\boldsymbol{N}\boldsymbol{q}_e, a, b)$ is the at least p-times differentiable step function defined in 3.2 with $p \geq 3$. The constants a and b are chosen such that

$$0 \leq a < b < \mu \tag{24}$$

Remark 6.1 The function V_1 is a class $\mathcal{K}_\infty$ function of $\| \boldsymbol{q}_e \|$ and $\| \boldsymbol{p}_e \|$, and tends to infinity when $\boldsymbol{q}_e^{\mathrm{T}}\boldsymbol{N}\boldsymbol{q}_e$ tends to μ. Moreover, the use of $h(\boldsymbol{q}_e^{\mathrm{T}}\boldsymbol{N}\boldsymbol{q}_e, a, b)$ is to ensure that V_1 takes care of the constraints on $\boldsymbol{q}_e$ only when $\boldsymbol{q}_e^{\mathrm{T}}\boldsymbol{N}\boldsymbol{q}_e$ is sufficiently close to its constraint μ. This also means that when $\boldsymbol{q}_e^{\mathrm{T}}\boldsymbol{N}\boldsymbol{q}_e$ is sufficiently less than their constraints, V_1 does not put a weight on these errors to reduce the control effort.

Differentiating both sides of (21) along the solutions of (20) and (19) gives

$$\begin{aligned} V_1 = \\ &\boldsymbol{p}_e^{\mathrm{T}}\{\boldsymbol{K}_1\sigma(\boldsymbol{q}_e) + 2\beta'\boldsymbol{N}\boldsymbol{q}_e - (d_{v1}^{\diamond} + f_2^{\diamond}(v))\boldsymbol{p}_e + \boldsymbol{C}_l((\varepsilon-1)r)\boldsymbol{p}_d + \\ &\begin{bmatrix} \cos(\psi)\tau_u^{\diamond} \\ \sin(\psi)\tau_u^{\diamond} \end{bmatrix} + \frac{1}{m_{22}}\begin{bmatrix} \hat{\theta}_1 \\ \hat{\theta}_2 \end{bmatrix} - (d_{v1}^{\diamond} + f_2^{\diamond}(v))\boldsymbol{p}_d - \dot{\vartheta}_d \begin{bmatrix} \cos(\psi_d) \\ \sin(\psi_d) \end{bmatrix} - \\ &\dot{\psi}_d \begin{bmatrix} -\dot{y}_d \\ \dot{x}_d \end{bmatrix}\} + \boldsymbol{p}_e^{\mathrm{T}}(F\tau_u^{\diamond} + \boldsymbol{J}_l(\psi)\boldsymbol{M}_l^{-1}\boldsymbol{J}_l^{-1}(\psi)\tilde{\theta}_{12}) \end{aligned} \tag{25}$$

where $\beta' = \dfrac{\partial\beta}{\partial(\boldsymbol{q}_e^{\mathrm{T}}\boldsymbol{N}\boldsymbol{q}_e)}$, we have used $\boldsymbol{p}_e^{\mathrm{T}}\boldsymbol{C}_l((\varepsilon-1)r)\boldsymbol{p}_e = 0$, and

$$\begin{aligned} &F = \mathrm{col}(\Phi_1, \Phi_2), \ \tilde{\theta}_{12} = \mathrm{col}(\tilde{\theta}_1, \tilde{\theta}_2) \\ &\Phi_1 = (\cos(\psi_e) - 1)\cos(\alpha_\psi) - \sin(\psi_e)\sin(\alpha_\psi) \\ &\Phi_2 = \sin(\psi_e)\cos(\alpha_\psi) + (\cos(\psi_e) - 1)\sin(\alpha_\psi) \end{aligned} \tag{26}$$

We cannot use the controls α_ψ and $\tau_u^{\diamond}$ to cancel the term $\boldsymbol{C}_l((\varepsilon-1)r)\boldsymbol{p}_d$ because canceling this term will result in a "pre-mature" control problem in the next step. To resolve this problem, we choose the controls α_ψ and $\tau_u^{\diamond}$ as follows

$$\begin{aligned} \begin{bmatrix} \cos(\alpha_\psi)\tau_u^{\diamond} \\ \sin(\alpha_\psi)\tau_u^{\diamond} \end{bmatrix} = &-\boldsymbol{K}_1\sigma(\boldsymbol{q}_e) - 2\beta'\boldsymbol{N}\boldsymbol{q}_e - \frac{1}{m_{22}}\begin{bmatrix} \hat{\theta}_1 \\ \hat{\theta}_2 \end{bmatrix} + \dot{\psi}_d \begin{bmatrix} -\dot{y}_d \\ \dot{x}_d \end{bmatrix} - \\ &\boldsymbol{C}_l((\varepsilon-1)\delta_d)\boldsymbol{p}_d + (d_{v1}^{\diamond} + f_2^{\diamond}(v))\boldsymbol{p}_d + \dot{\vartheta}_d \begin{bmatrix} \cos(\psi_d) \\ \sin(\psi_d) \end{bmatrix} \end{aligned} \tag{27}$$

where we have introduced a variable δ_d determined later to overcome the pre-mature control problem as mentioned above. We now solve (27) for α_ψ and $\tau_u^{\diamond}$. Multiplying both sides of the first and second equations of (27) by $\cos(\psi_d)$ and $\sin(\psi_d)$, respectively, then adding them together, and multiplying both sides of the first and second equations of (27) by $\sin(\psi_d)$ and $\cos(\psi_d)$, respectively, then subtracting them from each other result in

$$\begin{aligned} &\cos(\alpha_\psi - \psi_d)\tau_u^{\diamond} = \dot{\vartheta}_d + (d_{v1}^{\diamond} + f_2^{\diamond}(v))\vartheta_d - \frac{1}{m_{22}}(\hat{\theta}_1\cos(\psi_d) + \\ &\quad \hat{\theta}_2\sin(\psi_d)) - (k_{11}\cos(\psi_d)\sigma(x_e) + k_{12}\sin(\psi_d)\sigma(y_e)) - \\ &\quad (\varpi_{xe}\cos(\psi_d) + \varpi_{ye}\sin(\psi_d)) := B \\ &\sin(\alpha_\psi - \psi_d)\tau_u^{\diamond} = \dot{\psi}_d\vartheta_d - \frac{1}{m_{22}}(-\hat{\theta}_1\sin(\psi_d) + \hat{\theta}_2\cos(\psi_d)) - \\ &\quad (-k_{11}\sin(\psi_d)\sigma(x_e) + k_{12}\cos(\psi_d)\sigma(y_e)) - \\ &\quad (-\varpi_{xe}\sin(\psi_d) + \varpi_{ye}\cos(\psi_d)) - (1-\varepsilon)\delta_d\vartheta_d := A \end{aligned} \tag{28}$$

where ϖ_{xe} and ϖ_{ye} are the first and second elements of $2\beta' \boldsymbol{N}\boldsymbol{q}_e$, respectively, i.e., $2\beta' \boldsymbol{N}\boldsymbol{q}_e = \mathrm{col}(\varpi_{xe}, \varpi_{ye})$. To ensure smooth controls α_ψ and $\tau_u^\diamond$ can be obtained by solving (28), we choose

$$\begin{aligned} \dot{\vartheta}_d &= -(d_{v1}^\diamond + f_2^\diamond(v))\vartheta_d + \sqrt{\varepsilon_0^2 + L^2} + \Lambda_d(t) \\ \vartheta_d(t_0) &= \vartheta_{d0} \end{aligned} \tag{29}$$

where ε_0 is an arbitrarily small positive constant, ϑ_{d0} is a positive constant, L is given by

$$L = -(\varpi_{xe}\cos(\psi_d) + \varpi_{ye}\sin(\psi_d)) \tag{30}$$

and $\Lambda_d(t)$ is a bounded, positive and twice differentiable function of time t and satisfies the following condition:

$$\begin{aligned} \Lambda_d(t) \geq k_{11} + k_{12} + \frac{1}{m_{22}}(\max(|\theta_1^{\min}|, |\theta_1^{\max}|) + \\ \max(|\theta_2^{\min}|, |\theta_2^{\max}|)) + \Lambda_d^{\min} \end{aligned} \tag{31}$$

where $\Lambda_d^{\min}$ is a strictly positive constant. It is noted that with the help of the controller proposed in sequel the sway velocity v will converge to some desired sway velocity v_d, and Γ will converge to zero, the function $\Lambda_d(t)$ plays the role of specifying the desired velocity ϑ_d at the steady state. The update law for the path parameter s is found by using $\vartheta_d = \sqrt{x_{d'}^2 + y_{d'}^2}\,\dot{s}$, see (16), once ϑ_d is available from (29). Since ϑ_d is chosen such that (29) holds, we have

$$B \geq \Lambda_d^{\min} \tag{32}$$

because the disturbance observer (10) guarantees that $\hat{\theta}_i(t) \in [\theta_i^{\min}, \theta_i^{\max}]$, $i = 1,2,3$, see (11). Thus, smooth controls α_ψ and $\tau_u^\diamond$ can be obtained by solving (28) as follows

$$\begin{aligned} \alpha_\psi &= \psi_d + \arctan(A/B) \\ \tau_u^\diamond &= A\sin(\alpha_\psi - \psi_d) + B\cos(\alpha_\psi - \psi_d) \end{aligned} \tag{33}$$

The variable δ_d will be determined in the next step. Substituting (33) or (27) into (25) yields

$$\begin{aligned} \dot{V}_1 = -\boldsymbol{p}_e^{\mathrm{T}}(d_{v1}^\diamond + f_2^\diamond(v))\boldsymbol{p}_e + \boldsymbol{p}_e^{\mathrm{T}}(\boldsymbol{C}_l((\varepsilon-1)r) - \\ \boldsymbol{C}_l((\varepsilon-1)\delta_d))\boldsymbol{p}_d + \boldsymbol{p}_e^{\mathrm{T}}(F\tau_u^\diamond + \boldsymbol{J}_l(\psi)\boldsymbol{M}_l^{-1}\boldsymbol{J}_l^{-1}(\psi)\tilde{\theta}_{12}) \end{aligned} \tag{34}$$

On the other hand, substituting (27) into (19) gives

$$\begin{aligned} \dot{\boldsymbol{q}}_e &= \boldsymbol{p}_e \\ \dot{\boldsymbol{p}}_e &= \boldsymbol{C}_l((\varepsilon-1)r)\boldsymbol{p}_e - (d_{v1}^\diamond + f_2^\diamond(v))\boldsymbol{p}_e + \\ &\quad \boldsymbol{C}_l((\varepsilon-1)r)\boldsymbol{p}_d - \boldsymbol{C}_l((\varepsilon-1)\delta_d)\boldsymbol{p}_d - \boldsymbol{K}_1\sigma(\boldsymbol{q}_e) - \\ &\quad 2\beta'\boldsymbol{N}\boldsymbol{q}_e + F\tau_u^\diamond + \boldsymbol{J}_l(\psi)\boldsymbol{M}_l^{-1}\boldsymbol{J}_l^{-1}(\psi)\tilde{\theta}_{12} \end{aligned} \tag{35}$$

6.2 Step 2

Define

$$r_e = r - \alpha_r \tag{36}$$

where α_r is a virtual control of r. Due to (29), we have the fact that α_ψ and $\tau_u^\diamond$ are smooth functions of $(\psi_d, \dot{\psi}_d, \hat{\theta}_1, \hat{\theta}_2, \boldsymbol{q}_e, \delta_d, \Lambda_d)$. Thus, differentiating both sides of (20) along the solutions of (36), the first equation of (35), and the third equation of (14) results in

$$\begin{aligned} \dot{\psi}_e = r_e + \alpha_r - \frac{\partial\alpha_\psi}{\partial\psi_d}\dot{\psi}_d - \frac{\partial\alpha_\psi}{\partial\dot{\psi}_d}\ddot{\psi}_d + k_{01}\frac{\partial\alpha_\psi}{\partial\hat{\theta}_1}\tilde{\theta}_1 + \\ k_{02}\frac{\partial\alpha_\psi}{\partial\hat{\theta}_2}\tilde{\theta}_2 - \frac{\partial\alpha_\psi}{\partial\boldsymbol{q}_e}\boldsymbol{p}_e - \frac{\partial\alpha_\psi}{\partial\delta_d}\dot{\delta}_d - \frac{\partial\alpha_\psi}{\partial\Lambda_d}\dot{\Lambda}_d \end{aligned} \tag{37}$$

where we have used the fact that $\dot{\hat{\theta}}_i = -\dot{\tilde{\theta}}_i = k_{0i}\tilde{\theta}_i$, see (12). To design α_r, we consider the Lyapunov function candidate:

$$V_2 = V_1 + \frac{1}{2}\psi_e^2 \tag{38}$$

whose derivative along the solutions of (37) and (34) is

$$\begin{aligned} \dot{V}_2 &= -\boldsymbol{p}_e^{\mathrm{T}}(d_{v1}^\diamond + f_2^\diamond(v))\boldsymbol{p}_e + \boldsymbol{p}_e^{\mathrm{T}}(\boldsymbol{C}_l((\varepsilon-1)r) - \\ &\quad \boldsymbol{C}_l((\varepsilon-1)\delta_d))\boldsymbol{p}_d + \boldsymbol{p}_e^{\mathrm{T}}\boldsymbol{J}_l(\psi)\boldsymbol{M}_l^{-1}\boldsymbol{J}_l^{-1}(\psi)\tilde{\theta}_{12} + \\ &\quad \psi_e\Big(F^\diamond\tau_u^\diamond + r_e + \alpha_r - \frac{\partial\alpha_\psi}{\partial\psi_d}\dot{\psi}_d - \frac{\partial\alpha_\psi}{\partial\dot{\psi}_d}\ddot{\psi}_d + k_{01}\frac{\partial\alpha_\psi}{\partial\hat{\theta}_1}\tilde{\theta}_1 + \\ &\quad k_{02}\frac{\partial\alpha_\psi}{\partial\hat{\theta}_2}\tilde{\theta}_2 - \frac{\partial\alpha_\psi}{\partial\boldsymbol{q}_e}\boldsymbol{p}_e - \frac{\partial\alpha_\psi}{\partial\delta_d}\dot{\delta}_d - \frac{\partial\alpha_\psi}{\partial\Lambda_d}\dot{\Lambda}_d\Big) \end{aligned} \tag{39}$$

where $F^\diamond = F/\psi_e$, which is well-defined because $(\cos(\psi_e)-1)/\psi_e$ and $\sin(\psi_e)/\psi_e$ are smooth functions of ψ_e, see (26) for the expression of F. From (39), we choose α_r as follows:

$$\begin{aligned} \alpha_r = -k_2\psi_e - F^\diamond\tau_u^\diamond + \frac{\partial\alpha_\psi}{\partial\psi_d}\dot{\psi}_d + \frac{\partial\alpha_\psi}{\partial\dot{\psi}_d}\ddot{\psi}_d + \\ \frac{\partial\alpha_\psi}{\partial\boldsymbol{q}_e}\boldsymbol{p}_e + \frac{\partial\alpha_\psi}{\partial\delta_d}\dot{\delta}_d + \frac{\partial\alpha_\psi}{\partial\Lambda_d}\dot{\Lambda}_d \end{aligned} \tag{40}$$

where k_2 is a positive constant. Substituting (40) and (36) into (39) results in

$$\begin{aligned} \dot{V}_1 &= -\boldsymbol{p}_e^{\mathrm{T}}(d_{v1}^\diamond + f_2^\diamond(v))\boldsymbol{p}_e - k_2\psi_e^2 + (\boldsymbol{p}_e^{\mathrm{T}}\boldsymbol{C}_l(\varepsilon-1)\boldsymbol{p}_d + \psi_e)r_e + \\ &\quad \boldsymbol{p}_e^{\mathrm{T}}(\boldsymbol{C}_l((\varepsilon-1)\alpha_r) - \boldsymbol{C}_l((\varepsilon-1)\delta_d))\boldsymbol{p}_d + \\ &\quad \boldsymbol{p}_e^{\mathrm{T}}\boldsymbol{J}_l(\psi)\boldsymbol{M}_l^{-1}\boldsymbol{J}_l^{-1}(\psi)\tilde{\theta}_{12} + \psi_e(k_{01}\frac{\partial\alpha_\psi}{\partial\hat{\theta}_1}\tilde{\theta}_1 + k_{02}\frac{\partial\alpha_\psi}{\partial\hat{\theta}_2}\tilde{\theta}_2) \end{aligned} \tag{41}$$

We now determine a dynamical system that generates δ_d

to make the term $\boldsymbol{p}_e^{\mathrm{T}}(\boldsymbol{C}_l((\varepsilon-1)\alpha_r)-\boldsymbol{C}_l((\varepsilon-1)\delta_d))\boldsymbol{p}_d$ in (41) equal to zero. Since $\boldsymbol{p}_e^{\mathrm{T}}(\boldsymbol{C}_l((\varepsilon-1)\alpha_r)-\boldsymbol{C}_l((\varepsilon-1)\delta_d))\boldsymbol{p}_d=0$ if $\alpha_r=\delta_d$. Using α_r given in (40), the equation $\alpha_r=\delta_d$ is equivalent to

$$\dot{\delta}_d=\frac{1}{\dfrac{\partial\alpha_\psi}{\partial\delta_d}}\left(k_2\psi_e+F^{\diamondsuit}\tau_u^{\diamondsuit}-\frac{\partial\alpha_\psi}{\partial\psi_d}\dot{\psi}_d-\frac{\partial\alpha_\psi}{\partial\dot{\psi}_d}\ddot{\psi}_d-\frac{\partial\alpha_\psi}{\partial\boldsymbol{q}_e}\boldsymbol{p}_e-\frac{\partial\alpha_\psi}{\partial\Lambda_d}\dot{\Lambda}_d+\dot{\delta}_d\right) \tag{42}$$

We will prove in Appendix 9 that $\delta_d(t)$ is bounded. Substituting (42) into (41) yields

$$\dot{V}_2=-\boldsymbol{p}_e^{\mathrm{T}}(d_{v1}^{\diamondsuit}+f_2^{\diamondsuit}(v))\boldsymbol{p}_e-k_2\psi_e^2+(\boldsymbol{p}_e^{\mathrm{T}}\boldsymbol{C}_l((\varepsilon-1))\boldsymbol{p}_d+\psi_e)r_e+\boldsymbol{p}_e^{\mathrm{T}}\boldsymbol{J}_l(\psi)\boldsymbol{M}_l^{-1}\boldsymbol{J}_l^{-1}(\psi)\tilde{\theta}_{12}+\psi_e(k_{01}\frac{\partial\alpha_\psi}{\partial\hat{\theta}_1}\tilde{\theta}_1+k_{02}\frac{\partial\alpha_\psi}{\partial\hat{\theta}_2}\tilde{\theta}_2) \tag{43}$$

Moreover, substituting (27) and (42) into (19), and (40) and (42) into (37) gives

$$\begin{aligned}\dot{\boldsymbol{q}}_e&=\boldsymbol{p}_e\\ \dot{\boldsymbol{p}}_e&=\boldsymbol{C}_l((\varepsilon-1)r)\boldsymbol{p}_e-(d_{v1}^{\diamondsuit}+f_2^{\diamondsuit}(v))\boldsymbol{p}_e+\boldsymbol{C}_l((\varepsilon-1)r_e)\boldsymbol{p}_d-\\ &\quad\boldsymbol{K}_1\sigma(\boldsymbol{q}_e)-2\beta'\boldsymbol{N}\boldsymbol{q}_e+F\tau_u^{\diamondsuit}+\boldsymbol{J}_l(\psi)\boldsymbol{M}_l^{-1}\boldsymbol{J}_l^{-1}(\psi)\tilde{\theta}_{12}\\ \dot{\psi}_e&=r_e-k_2\psi_e-F^{\diamondsuit}\tau_u^{\diamondsuit}+k_{01}\frac{\partial\alpha_\psi}{\partial\hat{\theta}_1}\tilde{\theta}_1+k_{02}\frac{\partial\alpha_\psi}{\partial\hat{\theta}_2}\tilde{\theta}_2\end{aligned} \tag{44}$$

6.3 Step 3

Since α_r is a smooth function of $(\psi_d,\dot{\psi}_d,\ddot{\psi}_d,\ \hat{\theta}_1,\hat{\theta}_2,\ \boldsymbol{q}_e,\boldsymbol{p}_e,\ \delta_d,\dot{\delta}_d,\ \Lambda_d,\dot{\Lambda}_d)$, differentiating both sides of (36) along the solutions of (44), and the last equation of (14) results in

$$\begin{aligned}\dot{r}_e&=\frac{m_{11}-m_{22}}{m_{33}}uv-f_3(r)+\frac{\tau_r}{m_{33}}+\frac{\theta_3}{m_{33}}-\frac{\partial\alpha_r}{\partial\psi_d}\dot{\psi}_d-\frac{\partial\alpha_r}{\partial\dot{\psi}_d}\ddot{\psi}_d-\\ &\quad\frac{\partial\alpha_r}{\partial\ddot{\psi}_d}\dddot{\psi}_d+k_{01}\frac{\partial\alpha_r}{\partial\hat{\theta}_1}\tilde{\theta}_1+k_{02}\frac{\partial\alpha_r}{\partial\hat{\theta}_2}\tilde{\theta}_2-\frac{\partial\alpha_r}{\partial\boldsymbol{q}_e}\boldsymbol{p}_e-\\ &\quad\frac{\partial\alpha_r}{\partial\boldsymbol{p}_e}(\boldsymbol{C}_l((\varepsilon-1)r)\boldsymbol{p}_e-(d_{v1}^{\diamondsuit}+f_2^{\diamondsuit}(v))\boldsymbol{p}_e+\boldsymbol{C}_l((\varepsilon-1)r_e)\boldsymbol{p}_d-\\ &\quad\boldsymbol{K}_1\sigma(\boldsymbol{q}_e)-2\beta'\boldsymbol{N}\boldsymbol{q}_e+F\tau_u^{\diamondsuit}+\boldsymbol{J}_l(\psi)\boldsymbol{M}_l^{-1}\boldsymbol{J}_l^{-1}(\psi)\tilde{\theta}_{12})-\\ &\quad\frac{\partial\alpha_r}{\partial\delta_d}\dot{\delta}_d-\frac{\partial\alpha_r}{\partial\dot{\delta}_d}\dot{\delta}_d-\frac{\partial\alpha_r}{\partial\Lambda_d}\dot{\Lambda}_d-\frac{\partial\alpha_r}{\partial\dot{\Lambda}_d}\ddot{\Lambda}_d\end{aligned} \tag{45}$$

To design the control τ_r, we consider the following Lyapunov function candidate

$$V_3=V_2+\frac{1}{2}r_e^2 \tag{46}$$

whose derivative along the solutions of (43) and (45) is

$$\begin{aligned}\dot{V}_3&=-\boldsymbol{p}_e^{\mathrm{T}}(d_{v1}^{\diamondsuit}+f_2^{\diamondsuit}(v))\boldsymbol{p}_e-k_2\psi_e^2+(\boldsymbol{p}_e^{\mathrm{T}}\boldsymbol{C}_l(\varepsilon-1)\boldsymbol{p}_d+\psi_e)r_e+\\ &\quad\boldsymbol{p}_e^{\mathrm{T}}\boldsymbol{J}_l(\psi)\boldsymbol{M}_l^{-1}\boldsymbol{J}_l^{-1}(\psi)\tilde{\theta}_{12}+\psi_e(k_{01}\frac{\partial\alpha_\psi}{\partial\hat{\theta}_1}\tilde{\theta}_1+k_{02}\frac{\partial\alpha_\psi}{\partial\hat{\theta}_2}\tilde{\theta}_2)+\\ &\quad r_e[\frac{m_{11}-m_{22}}{m_{33}}uv-f_3(r)+\frac{\tau_r}{m_{33}}+\frac{\theta_3}{m_{33}}-\frac{\partial\alpha_r}{\partial\psi_d}\dot{\psi}_d-\\ &\quad\frac{\partial\alpha_r}{\partial\dot{\psi}_d}\ddot{\psi}_d-\frac{\partial\alpha_r}{\partial\ddot{\psi}_d}\dddot{\psi}_d+k_{01}\frac{\partial\alpha_r}{\partial\hat{\theta}_1}\tilde{\theta}_1+k_{02}\frac{\partial\alpha_r}{\partial\hat{\theta}_2}\tilde{\theta}_2-\frac{\partial\alpha_r}{\partial\boldsymbol{q}_e}\boldsymbol{p}_e-\\ &\quad\frac{\partial\alpha_r}{\partial\boldsymbol{p}_e}(\boldsymbol{C}_l((\varepsilon-1)r)\boldsymbol{p}_e-(d_{v1}^{\diamondsuit}+f_2^{\diamondsuit}(v))\boldsymbol{p}_e+\boldsymbol{C}_l((\varepsilon-1)r_e)\boldsymbol{p}_d-\\ &\quad\boldsymbol{K}_1\sigma(\boldsymbol{q}_e)-2\beta'\boldsymbol{N}\boldsymbol{q}_e+F\tau_u^{\diamondsuit}+\boldsymbol{J}_l(\psi)\boldsymbol{M}_l^{-1}\boldsymbol{J}_l^{-1}(\psi)\tilde{\theta}_{12})-\\ &\quad\frac{\partial\alpha_r}{\partial\delta_d}\dot{\delta}_d-\frac{\partial\alpha_r}{\partial\dot{\delta}_d}\dot{\delta}_d-\frac{\partial\alpha_r}{\partial\Lambda_d}\dot{\Lambda}_d-\frac{\partial\alpha_r}{\partial\dot{\Lambda}_d}\ddot{\Lambda}_d]\end{aligned} \tag{47}$$

From (47), we choose the control τ_r as follows

$$\begin{aligned}\tau_r&=m_{33}[-k_3r_e-\boldsymbol{p}_e^{\mathrm{T}}\boldsymbol{C}_l(\varepsilon-1)\boldsymbol{p}_d-\psi_e-\frac{m_{11}-m_{22}}{m_{33}}uv+\\ &\quad\frac{d_{r1}\alpha_r}{m_{33}}+f_3^{\diamondsuit}(r)\alpha_r-\frac{\hat{\theta}_3}{m_{33}}+\frac{\partial\alpha_r}{\partial\psi_d}\dot{\psi}_d+\frac{\partial\alpha_r}{\partial\dot{\psi}_d}\ddot{\psi}_d+\frac{\partial\alpha_r}{\partial\ddot{\psi}_d}\dddot{\psi}_d+\\ &\quad\frac{\partial\alpha_r}{\partial\boldsymbol{q}_e}\boldsymbol{p}_e+\frac{\partial\alpha_r}{\partial\boldsymbol{p}_e}(\boldsymbol{C}_l((\varepsilon-1)r)\boldsymbol{p}_e-(d_{v1}^{\diamondsuit}+f_2^{\diamondsuit}(v))\boldsymbol{p}_e+\\ &\quad\boldsymbol{C}_l((\varepsilon-1)r_e)\boldsymbol{p}_d-\boldsymbol{K}_1\sigma(\boldsymbol{q}_e)-2\beta'\boldsymbol{N}\boldsymbol{q}_e+F\tau_u^{\diamondsuit})+\frac{\partial\alpha_r}{\partial\delta_d}\dot{\delta}_d+\\ &\quad\frac{\partial\alpha_r}{\partial\dot{\delta}_d}\dot{\delta}_d+\frac{\partial\alpha_r}{\partial\Lambda_d}\dot{\Lambda}_d+\frac{\partial\alpha_r}{\partial\dot{\Lambda}_d}\ddot{\Lambda}_d-\rho_1(\frac{\partial\alpha_r}{\partial\hat{\theta}_1})^2r_e-\rho_2(\frac{\partial\alpha_r}{\partial\hat{\theta}_2})^2r_e-\\ &\quad\rho_3\|\frac{\partial\alpha_r}{\partial\boldsymbol{p}_e}\boldsymbol{J}_l(\psi)\boldsymbol{M}_l^{-1}\boldsymbol{J}_l^{-1}(\psi)\|^2{}_e]\end{aligned} \tag{48}$$

where k_3, ρ_1, ρ_2, and ρ_3 are positive constants. The last three terms in the right-hand side of (48) are nonlinear damping to handle the terms $r_e\frac{\partial\alpha_r}{\partial\hat{\theta}_1}\tilde{\theta}_1$, $r_e\frac{\partial\alpha_r}{\partial\hat{\theta}_2}\tilde{\theta}_2$, and $r_e\frac{\partial\alpha_r}{\partial\boldsymbol{p}_e}\boldsymbol{J}_l(\psi)\boldsymbol{M}_l^{-1}\boldsymbol{J}_l^{-1}(\psi)\tilde{\theta}_{12}$ in the right-hand side of (47). Substituting (48) into (47) gives

$$\begin{aligned}\dot{V}_3&=-\boldsymbol{p}_e^{\mathrm{T}}(d_{v1}^{\diamondsuit}+f_2^{\diamondsuit}(v))\boldsymbol{p}_e-k_2\psi_e^2-(k_3+\frac{d_{r1}}{m_{33}}+f_3^{\diamondsuit}(r))r_e^2+\\ &\quad\boldsymbol{p}_e^{\mathrm{T}}\boldsymbol{J}_l(\psi)\boldsymbol{M}_l^{-1}\boldsymbol{J}_l^{-1}(\psi)\tilde{\theta}_{12}+\psi_e(k_{01}\frac{\partial\alpha_\psi}{\partial\hat{\theta}_1}\tilde{\theta}_1+k_{02}\frac{\partial\alpha_\psi}{\partial\hat{\theta}_2}\tilde{\theta}_2)+\\ &\quad r_e\left[\frac{\tilde{\theta}_3}{m_{33}}+k_{01}\frac{\partial\alpha_r}{\partial\hat{\theta}_1}\tilde{\theta}_1+k_{02}\frac{\partial\alpha_r}{\partial\hat{\theta}_2}\tilde{\theta}_2+\frac{\partial\alpha_r}{\partial\boldsymbol{p}_e}\boldsymbol{J}_l(\psi)\boldsymbol{M}_l^{-1}\boldsymbol{J}_l^{-1}(\psi)\tilde{\theta}_{12}\right]-\\ &\quad\rho_1(\frac{\partial\alpha_r}{\partial\hat{\theta}_1})^2r_e^2-\rho_2(\frac{\partial\alpha_r}{\partial\hat{\theta}_2})^2r_e^2-\rho_3\|\frac{\partial\alpha_r}{\partial\boldsymbol{p}_e}\boldsymbol{J}_l(\psi)\boldsymbol{M}_l^{-1}\boldsymbol{J}_l^{-1}(\psi)\|^2r_e^2\end{aligned} \tag{49}$$

Moreover, substituting (48) into (45) yields

$$\dot{r}_e = (k_3 + \frac{d_{r1}}{m_{33}} + f_3^{\diamond}(r))r_e + \frac{\tilde{\theta}_3}{m_{33}} + k_{01}\frac{\partial \alpha_r}{\partial \hat{\theta}_1}\tilde{\theta}_1 + k_{02}\frac{\partial \alpha_r}{\partial \hat{\theta}_2}\tilde{\theta}_2 - \frac{\partial \alpha_r}{\partial \boldsymbol{p}_e}\boldsymbol{J}_l(\psi)\boldsymbol{M}_l^{-1}\boldsymbol{J}_l^{-1}(\psi)\tilde{\theta}_{12} - \rho_1(\frac{\partial \alpha_r}{\partial \hat{\theta}_1})^2 r_e - \rho_2(\frac{\partial \alpha_r}{\partial \hat{\theta}_2})^2 r_e - \rho_3 \| \frac{\partial \alpha_r}{\partial \boldsymbol{p}_e}\boldsymbol{J}_l(\psi)\boldsymbol{M}_l^{-1}\boldsymbol{J}_l^{-1}(\psi) \|^2 r_e \tag{50}$$

The control design has been completed. We present the main results in Theorem 6.1.

Theorem 6.1 Under Assumption 2.1, the control inputs τ_u given by (13) with $\tau_u^{\diamond}$ designed as in (33) and τ_r given in (48), and the disturbance observer given in (10) solve the control objective 2.1. In particular, the following results hold:

1) The closed-loop system consists of (10), (29), (42), (44), and (50) is forward complete.

2) The ship is always within the constrained distance from the reference trajectory, i.e., the inequality (7) holds for all $t \geq t_0 \geq 0$. This does not depend on the convergence of the disturbance observer as the stability analysis is carried out for all signals of the closed-loop system.

3) The tracking errors $(\boldsymbol{q}_e(t), \boldsymbol{p}_e(t), \psi_e(t), r_e(t))$ asymptotically converge to zero. Convergence of $\psi_e(t)$ to zero implies from (20) and (33) that of $\psi(t)$ to $\psi_d + \arctan(A/B)|_{\boldsymbol{q}_e=0}$. The angle $\arctan(A/B)|_{\boldsymbol{q}_e=0, \boldsymbol{p}_e=0}$, which is bounded, is for compensation of relaxation of the reference path generation and the sea load.

4) The function $\delta_d(t)$ generated by (42) is bounded for all $t \geq t_0 \geq 0$.

5) The desired total linear velocity coordinated in the earth-fixed frame is obtained by specifying the function $\Lambda_d(t)$ in (29).

Proof. See Appendix A.

7 Simulations

This section illustrates the effectiveness of the control design proposed in the previous section by simulating it on a monohull ship with the length of 32 m, mass of 118×10^3 kg. Other parameters are calculated by using MARINTEK Ship Motion program version 3.18, a program for calculating the added mass and damping matrices of the ship as:

$$m_{11} = 120\times10^3 \text{kg},\ m_{22} = 177.9\times10^3 \text{kg},\ m_{33} = 636\times10^5 \text{kg}\cdot\text{m}^2$$
$$d_{u1} = 215\times10^2 \text{kg}\cdot\text{s}^{-1},\ d_{u2} = 43\times10^2 \text{kg}\cdot\text{m}^{-1}$$
$$d_{u3} = 21.5\times10^2 \text{kg}\cdot\text{s}\cdot\text{m}^{-2},\ d_{v1} = 117\times10^3 \text{kg}\cdot\text{s}^{-1}$$
$$d_{v2} = 23.4\times10^3 \text{kg}\cdot\text{m}^{-1},\ d_{v3} = 11.7\times10^3 \text{kg}\cdot\text{s}\cdot\text{m}^{-2}$$
$$d_{r1} = 802\times10^4 \text{kg}\cdot\text{m}^2\cdot\text{s}^{-1},\ d_{r2} = 160.4\times10^4 \text{kg}\cdot\text{m}^2$$
$$d_{r3} = 80.2\times10^4 \text{kg}\cdot\text{m}^2\cdot\text{s},\ d_{ui} = 0,\ d_{vi} = 0,\ d_{ri} = 0$$

for all $i > 3$. In the simulations, we assume that the sea loads are such that: $\theta_1 = m_{11}$, $\theta_2 = m_{22}$, $\theta_3 = 0.5m_{33}$. The control gains are chosen as follows: $\theta_i^{\min} = 0$ and $\theta_i^{\max} = 1.2\theta_i$, $i = 1,2,3$, $\varepsilon_0 = 0.01$, $\boldsymbol{K}_0 = 2\boldsymbol{I}_2$ with $\boldsymbol{I}_2$ being the 2×2 identity matrix, $\boldsymbol{K}_1 = \boldsymbol{I}_2$, $k_2 = 2$, and $k_3 = 5$. The reference path is chosen to be a sinusoidal curve: $G(s) = \text{col}(s, R\sin(as))$ with $R = 15$ and $a = 0.02$. The initial values $s(0)$ and ϑ_{d0}, and function Λ_d are chosen as $s(0) = 0$, $\vartheta_{d0} = 4$ m/s and $\Lambda_d = 4$ m/s. The initial conditions are $x(0) = -15$ m, $y(0) = 15$ m, $\psi(0) = 0.5$ rad, $u(0) = 5$ m/s, $v(0) = 5$ m/s, and $r(0) = 2$ rad/s. The high initial velocities are chosen to illustrate the tracking error constraint. The constrained constants are chosen as $\boldsymbol{N} = \boldsymbol{I}_2$, $\mu = 470$, $b = \mu/2$, and $a = b/2$. Note that $\mu > \| \boldsymbol{q}_e(0) \|^2 = 450$. Excellent path-tracking results are plotted in Fig. 2.

It is particularly noted in Figs. 2(c) and 2(d) that the tracking error norm $d_e = \| \boldsymbol{q}_e \|$ is always less than $\sqrt{\mu} = 21.7$ and that $|\delta_d(t)|$ is bounded for all $t \geq 0$. In order to illustrate the effectiveness of the proposed controller, we also provide simulation results without the constraint, i.e., the matrix $\boldsymbol{N}$ is set to zero. Simulation results in this case are plotted in Fig. 3. Although excellent tracking results are obtained, the transient tracking error norm is much larger than in the case with the constraint ($\sup_{t\geq0} d_e(t) \approx 29$). It is noted that the path-tracking controllers proposed in (Lapierre and Jouvencel, 2008; Do and Pan, 2006; Ghommam *et al*., 2008) will give similar results because no hard-constraints on the tracking errors were addressed in these papers.

To demonstrate the performance improvement of the proposed path-tracking controller in this paper over the existing results, we perform a simulation on the trajectory-tracking controller proposed in (Do *et al*., 2002a). We do not provide a simulation on the path-following controllers proposed in (Skjetne and Fossen, 2001; Encarnação *et al*., 2000; Do and Pan, 2004; Li *et al*., 2009), for example, because these controllers are local as mentioned in Section 1. The framework of the trajectory-tracking control design for an underactuated ship is described in Fig. 4, where the control objective is to design the controls τ_u and τ_r to force the real ship to track the virtual ship. In Fig. 4, (x_d, y_d, ψ_d) represent position and orientation of the virtual ship with respect to the Earth-fixed frame $O_E X_E Y_E$, (u_d, v_d, r_d) are velocities of the virtual ship with respect to the virtual ship body-fixed frame $O_d X_d Y_d$. The virtual ship "dynamics" are given by

$$\dot{\eta}_d = \boldsymbol{J}(\psi_d)\boldsymbol{v}_d, \quad \dot{\boldsymbol{v}}_d = \boldsymbol{f}_d(\boldsymbol{v}_d) + \boldsymbol{M}^{-1}\tau_d \tag{51}$$

where

$$\eta_d = \mathrm{col}(x_d, y_d, \psi_d), \quad \boldsymbol{v}_d = \mathrm{col}(u_d, v_d, r_d)$$

$$\boldsymbol{J}(\psi_d) = \boldsymbol{J}(\psi)\big|_{\psi=\psi_d}$$

$$\boldsymbol{f}_d(\boldsymbol{v}_d) = \mathrm{col}\left(\frac{m_{22}}{m_{11}} v_d r_d, -\frac{m_{11}}{m_{22}} u_d r_d, \frac{m_{11}-m_{22}}{m_{33}} u_d v_d\right)$$

$$\tau_d = \mathrm{col}(\tau_{ud}, 0, \tau_{rd})$$

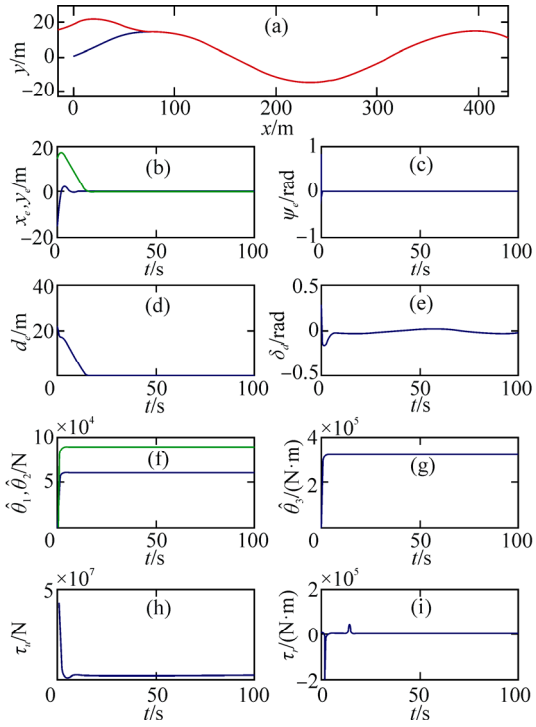

Fig. 2 Simulation results with tracking error constraint

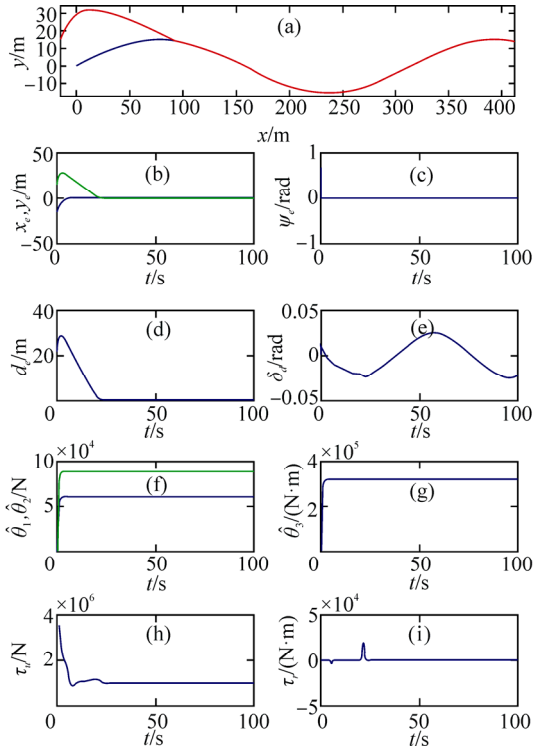

Fig. 3 Simulation results without tracking error constraint

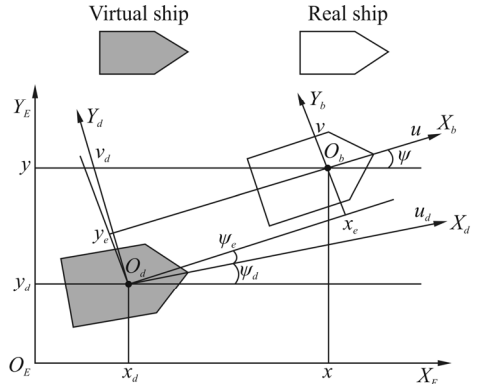

Fig. 4 Trajectory-tracking control design framework

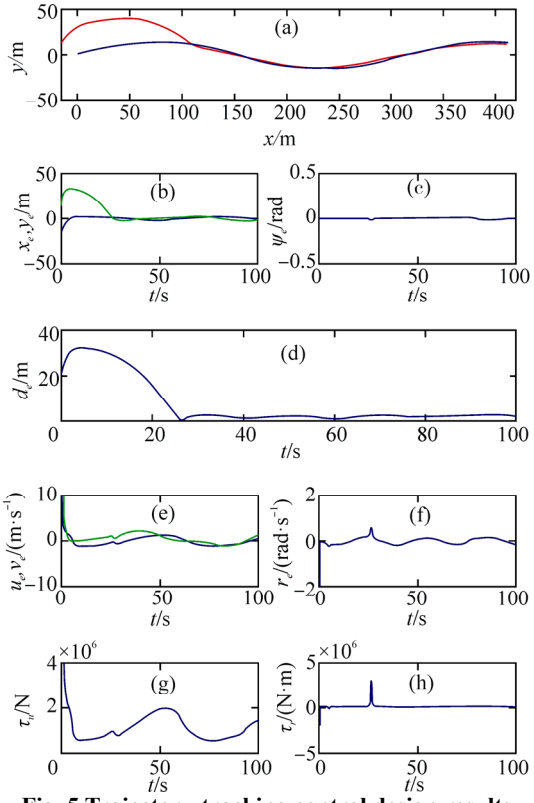

Fig. 5 Trajectory-tracking control design results

To generate (x_d, y_d, ψ_d), we specify $u_d = 4$ m/s and the profile of (x_d, y_d) in the Earth-fixed frame, i.e., the sinusoidal form of the aforementioned reference path. From these specifications, the reference inputs τ_{ud} and τ_{rd}. These in turn determine the reference trajectory (x_d, y_d, ψ_d). The errors in position and orientation between the real and virtual ships projected to the body-fixed frame $O_b X_b Y_b$ are denoted by (x_e, y_e, ψ_e). Thus, the trajectory-tracking control objective becomes the one of stabilizing the errors (x_e, y_e, ψ_e) at the origin, see (Do *et al*., 2002a) or (Lefeber *et al*., 2003; Do *et al*., 2002b; Lee and Jiang, 2004; Chwa, 2011) for details of trajectory-tracking control designs. The control gains are tuned so that the transient response time is almost the same

with the one simulated using the controller proposed in this paper for a fair comparison. The simulation results are plotted in Fig. 5, where the position and orientation tracking errors are plotted in Figs. 5(b) and 5(c); the norm of position tracking error is plotted in Fig. 5(d); the velocity tracking errors are plotted in Figs. 5(e) and 5(f); and the control inputs are plotted in Figs. 5(g) and 5(h). It is seen that the trajectory-tracking controller in (Do *et al*., 2002a) results in fairly large (steady state) tracking errors and more importantly the transient tracking error norm is much larger than the one proposed in this paper ($\sup_{t\geq 0} d_e(t) \approx 32.3$ vs $\sup_{t\geq 0} d_e(t) \approx 20.6$), see Fig. 5(d) vs Fig. 2(d). The large tracking errors are due to the fact that the controller in (Do *et al*., 2002a) was designed for the case without disturbance and nonlinear damping terms, with no hard constraint on tracking errors. It is noted that the trajectory-tracking controllers proposed in (Lefeber *et al*., 2003; Do *et al*., 2002b; Lee and Jiang, 2004; Chwa, 2011), for example, will give a similar transient response.

8 Conclusions

A constructive design of new controllers has been developed for path-tracking control of underactuated ships under sea loads and tracking error constraints. The keys to the successful control design include 1) a global exponential disturbance observer, 2) transformation of the ship dynamics to those of an almost spherical ship to almost decouple linear and angular motions of the ship, 3) the use of backstepping and Lyapunov's direct methods to stabilize the tracking errors expressed in the earth-fixed frame, and the introduction of an auxiliary function for compensation of relaxing the reference path generation. Future work will design an inverse optimal path-tracking controller for underactuated ships and path-tracking controllers for underwater vehicles based on the method proposed in this paper and the one in (Do, 2015).

Acknowledgments

The author would like to express his sincere gratitude to the Editor in Chief and the reviewers for their helpful comments. The work presented in this paper was supported in part by the Australian Research Council under grant DP0988424.

Appendix A: Proof of Theorem 6.1

A.1 Forward completeness of the closed-loop system

To prove forward completeness of the closed loop system, we consider the Lyapunov function candidate $V_\Sigma = V_3 + \frac{1}{2}\|\tilde{\theta}\|^2 + \frac{1}{2}\delta_d^2 + \frac{1}{2}\vartheta_d^2$, whose derivative along the solutions of (12), (42), (29), and (49) satisfies $\dot{V}_\Sigma \leq c_1 V_\Sigma + c_2$, where c_1 and c_2 are some positive constant. The above inequality together with the expression of V_Σ ensures that the closed-loop is forward complete. This proves Item 1) of Theorem 6.1.

A.2 Ship within the constrained distance

Since we have already proved that the closed-loop system is forward complete, we now can consider the closed-loop subsystem consisting of (12), (44) and (50) separately from the rest of the closed-loop system. As such, we consider the following Lyapunov function candidate

$$W = V_3 + 0.5c_3\|\tilde{\theta}\|^2 \tag{A1}$$

where c_3 is a positive constant to be picked. On the other hand, from (33) with A and B defined in (28) we have $\|\frac{\partial \alpha_\psi}{\partial \hat{\theta}_1}\| \leq \frac{2}{m_{22}\Lambda_d^{\min}}$, and $\|\frac{\partial \alpha_\psi}{\partial \hat{\theta}_2}\| \leq \frac{2}{m_{22}\Lambda_d^{\min}}$. Applying these bounds and the Young inequality to the derivative of W along the solutions of (12) and (49) results in

$$\begin{aligned} \dot{W} \leq & -(d_{v1}^{\diamond} - \varepsilon_1)\|\boldsymbol{p}_e\|^2 - (k_2 - 2\varepsilon_2)\psi_e^2 - \\ & (k_3 + d_{r1}/m_{33} - \varepsilon_3)r_e^2 - c_3^{\diamond}\|\tilde{\theta}\|^2 \end{aligned} \tag{A2}$$

where ε_1, ε_2, and ε_3 are positive constants to be picked, and

$$\begin{aligned} c_3^{\diamond} = & c_3\lambda_{\min}(\boldsymbol{K}_0) - \frac{1}{4\varepsilon_1 m_{11}} - \frac{(k_{01}^2 + k_{02}^2)}{\varepsilon_2 (m_{22}\Lambda_d^{\min})^2} - \\ & \frac{1}{4\varepsilon_3 m_{33}^2} - (\frac{1}{4\rho_1}k_{01}^2 + \frac{1}{4\rho_2}k_{02}^2 + \frac{1}{4\rho_3}) \end{aligned} \tag{A3}$$

with $\lambda_{min}(\bullet)$ is the minimum eigenvalue of $\bullet$. We pick sufficiently small ε_1, ε_2, ε_3, and sufficiently large c_3 such that $(d_{v1}^{\diamond} - \varepsilon_1)$, $(k_2 - 2\varepsilon_2)$, $(k_3 + \frac{d_{r1}}{m_{33}} - \varepsilon_3)$, and $c_3^{\diamond}$ are strictly positive. Then, we can write (A2) as $\dot{W} \leq 0$. Integrating $\dot{W} \leq 0$ from t_0 to t gives $W(t) \leq W(t_0)$. Substituting the detailed expression of W into $W(t) \leq W(t_0)$ results in

$$\begin{aligned} & \gamma(t) + \beta(t) + \frac{1}{2}\psi_e^2(t) + \frac{1}{2}r_e^2(t) + \frac{c_3}{2}\|\tilde{\theta}(t)\|^2 \leq \\ & \gamma(t_0) + \beta(t_0) + \frac{1}{2}\psi_e^2(t_0) + \frac{1}{2}r_e^2(t) + \frac{c_3}{2}\|\tilde{\theta}(t_0)\|^2 \end{aligned} \tag{A4}$$

where

$$\begin{aligned} \gamma(t) &= \int_0^{q_e(t)} \boldsymbol{\sigma}^{\mathrm{T}}(\chi)\boldsymbol{K}_1 d\chi + \frac{1}{2}\|\boldsymbol{p}_e(t)\|^2 \\ \beta(t) &= \frac{h(\boldsymbol{q}_e^{\mathrm{T}}(t)\boldsymbol{N}\boldsymbol{q}_e(t), a, b)\boldsymbol{q}_e^{\mathrm{T}}(t)\boldsymbol{N}\boldsymbol{q}_e(t)}{(\mu - h(\boldsymbol{q}_e^{\mathrm{T}}(t)\boldsymbol{N}\boldsymbol{q}_e(t), a, b)\boldsymbol{q}_e^{\mathrm{T}}(t)\boldsymbol{N}\boldsymbol{q}_e(t))^2} \end{aligned} \tag{A5}$$

Under the condition (6), the right-hand side of (A4) is bounded. Boundedness of the right-hand side of (A4) implies that the left-hand side of (A4) for all $t \geq t_0 \geq 0$. Boundedness of the left-hand side of (A4) means that $(\boldsymbol{q}_e(t), \boldsymbol{p}_e(t), \psi_e(t), r_e(t))$ are bounded and that $\mu - h(\boldsymbol{q}_e^{\mathrm{T}}(t)\boldsymbol{N}\boldsymbol{q}_e(t), a, b)\boldsymbol{q}_e^{\mathrm{T}}(t)\boldsymbol{N}\boldsymbol{q}_e(t)$ is larger than zero for

all $t \geq t_0 \geq 0$. This proves Item 2) of Theorem 6.1 since a and b are chosen as in (24).

A.3 Asymptotic convergence of tracking errors to zero

Since we have already proved that $(\boldsymbol{q}_e(t), \boldsymbol{p}_e(t), \psi_e(t), r_e(t))$ are bounded, $\mu - h(\boldsymbol{q}_e^{\mathrm{T}}(t)\boldsymbol{N}\boldsymbol{q}_e(t), a, b)\boldsymbol{q}_e^{\mathrm{T}}(t)\boldsymbol{N}\boldsymbol{q}_e(t)$ is larger than zero for all $t \geq t_0 \geq 0$, and $h(\boldsymbol{q}_e^{\mathrm{T}}(t)\boldsymbol{N}\boldsymbol{q}_e(t), a, b)$ is the p-times differentiable function of $\boldsymbol{q}_e$, a calculation from (29) that $\vartheta_d(t)$, $\dot{\vartheta}_d(t)$, and $\ddot{\vartheta}_d(t)$ are bounded for all $t \geq t_0 \geq 0$. Therefore, applying Theorem 4.4 in (Khalil, 2002) to (A2) yields

$$\lim_{t\to\infty}((d_{v1}^{\diamond} - \varepsilon_1)\| \boldsymbol{p}_e(t)\|^2 + (k_2 - 2\varepsilon_2)\psi_e^2(t) + (k_3 + \frac{d_{r1}}{m_{33}} - \varepsilon_3)r_e^2(t) + c_3^{\diamond}\| \tilde{\theta}(t)\|^2) = 0$$

which implies that $\lim_{t\to\infty}(\boldsymbol{p}_e(t), \psi_e(t), r_e(t), \tilde{\theta}(t)) = 0$. Moreover, applying the invariance principle (Theorem 4.4 in (Khalil, 2002)) to (44) yields

$$\begin{aligned}&\lim_{t\to\infty}(\boldsymbol{C}_l((\varepsilon-1)r(t))\boldsymbol{p}_e(t) - (d_{v1}^{\diamond} + f_2^{\diamond}(v(t)))\boldsymbol{p}_e(t) + \\ &\boldsymbol{C}_l((\varepsilon-1)r_e(t))\boldsymbol{p}_d(t) - \boldsymbol{K}_1\sigma(\boldsymbol{q}_e(t)) - 2\beta'(t)\boldsymbol{N}\boldsymbol{q}_e(t) + \\ &F(t)\tau_u^{\diamond} + \boldsymbol{J}_l(\psi(t))\boldsymbol{M}_l^{-1}\boldsymbol{J}_l^{-1}(\psi(t))\tilde{\theta}_{12}(t)) = 0\end{aligned} \quad \text{(A6)}$$

where we have abused the notation $F(t)$. Since $\lim_{t\to\infty}(\boldsymbol{p}_e(t), \psi_e(t), r_e(t), \tilde{\theta}(t)) = 0$ (as proved above), $\lim_{t\to\infty}F(t) = 0$, see (26) for the expression of F. This together with $\mathrm{col}(u, v) = \boldsymbol{J}_l^{-1}(\psi)\boldsymbol{p} = \boldsymbol{J}_l^{-1}(\psi)(\boldsymbol{p}_e + \boldsymbol{p}_d)$, ensures that the limit (A6) implies $\lim_{t\to\infty}(\boldsymbol{K}_1\sigma(\boldsymbol{q}_e(t)) + 2\beta'(\boldsymbol{q}_e(t))\boldsymbol{N}\boldsymbol{q}_e(t)) = 0$, which readily shows that $\lim_{t\to\infty}\boldsymbol{q}_e(t) = 0$ because $\beta'(\boldsymbol{q}_e(t)) > 0$ for all $t \geq t_0 \geq 0$.

A.4 Boundedness of $\delta_d(t)$

We first show that $\vartheta_d(t)$ is larger than a positive constant for all $t \geq t_0 \geq 0$. Since $\mathrm{col}(u, v) = \boldsymbol{J}_l^{-1}(\psi)\boldsymbol{p} = \boldsymbol{J}_l^{-1}(\psi)(\boldsymbol{p}_e + \boldsymbol{p}_d)$ and we have already proved that $\boldsymbol{p}_e(t)$ and $\vartheta_d(t)$ are bounded for all $t \geq t_0 \geq 0$, the differential equation (29) ensures that $\vartheta_d(t)$ is larger than a strictly positive constant. To show boundedness of $\delta_d(t)$ from (42), we first calculate the following partial derivatives:

$$\begin{aligned}&\frac{\partial\alpha_\psi}{\partial\delta_d} = \frac{-(1-\varepsilon)\vartheta_d}{A^2 + B^2} \\ &\frac{\partial\alpha_\psi}{\partial\psi_d} = 1 + \frac{\frac{\partial A}{\partial\psi_d}B - \frac{\partial B}{\partial\psi_d}A}{A^2 + B^2},\ \frac{\partial\alpha_\psi}{\partial\dot{\psi}_d} = \frac{\frac{\partial A}{\partial\dot{\psi}_d}B - \frac{\partial B}{\partial\dot{\psi}_d}A}{A^2 + B^2} \\ &\frac{\partial\alpha_\psi}{\partial\boldsymbol{q}_e} = \frac{\frac{\partial A}{\partial\boldsymbol{q}_e}B - \frac{\partial B}{\partial\boldsymbol{q}_e}A}{A^2 + B^2},\ \frac{\partial\alpha_\psi}{\partial\Lambda_d} = \frac{\frac{\partial A}{\partial\Lambda_d}B - \frac{\partial B}{\partial\Lambda_d}A}{A^2 + B^2}\end{aligned} \quad \text{(A7)}$$

From A and B defined in (28) and the fact that we have proved that $(\boldsymbol{q}_e(t), \boldsymbol{p}_e(t), \psi_e(t), r_e(t))$, $\vartheta_d(t)$ $\dot{\vartheta}_d(t)$, $\ddot{\vartheta}_d(t)$ are bounded, $\mu - h(\boldsymbol{q}_e^{\mathrm{T}}(t)\boldsymbol{N}\boldsymbol{q}_e(t), a, b)\boldsymbol{q}_e^{\mathrm{T}}(t)\boldsymbol{N}\boldsymbol{q}_e(t)$ is larger than zero for all $t \geq t_0 \geq 0$, and $\vartheta_d(t)$ is larger than a strictly positive constant, using (A7) it can be readily shown from (42) that $\delta_d(t)$ is bounded from all $t \geq t_0 \geq 0$ since $\varepsilon < 1$.

A.5 Specification of desired total linear velocity

By definition (16), we have $\boldsymbol{p}_d = \mathrm{col}(\vartheta_d\cos(\psi_d), \vartheta_d\sin(\psi_d))$. This means that the desired total linear velocity coordinated in the earth-fixed frame can be specified by specifying ϑ_d. Since ϑ_d is generated by (29), a proper choice of the function $\Lambda_d(t)$ will result in a desired ϑ_d. Moreover, we have already proved that $\lim_{t\to\infty}\boldsymbol{p}_e(t) = 0$ and recall that $\boldsymbol{p}_e = \boldsymbol{p} - \boldsymbol{p}_d$. Thus, at the steady state, the ship will move along the trajectory at the desired total linear velocity $\boldsymbol{p}_d$. Since $\lim_{t\to\infty}\psi_e(t) = 0$ as proved earlier, the ship's yaw angle converges to $\psi_d + \arctan(\frac{A}{B})|_{\boldsymbol{q}_e=0}$. The angle $\arctan(\frac{A}{B})|_{\boldsymbol{q}_e=0}$ is to compensate the loads θ_1 and θ_2, and the fact that the reference path $G(s)$ is not generated by a virtual ship. Finally, it is noted that since $B > 0$ for all $t \geq t_0 \geq 0$, the ship will not turn around.

References

Aguiar AP, Pascoal AM (2001). Regulation of a nonholonomic autonomous underwater vehicle with parametric modeling uncertainty using Lyapunov functions. *Proceedings of 40th IEEE Conference on Decision and Control*, Orlando, USA, **5**, 4178-4183.
DOI: 10.1109/.2001.980841

Aicardi M, Casalino G, Indiveri G, Aguiar A, Encarnação P, Pascoal A (2001). A planar path following controller for underactuated marine vehicles. *Proceedings of the Ninth IEEE Mediterranean Conference on Control and Automation*, Dubrovnik, Croatia, 1-6.

Brockett RW (1983). Asymptotic stability and feedback stabilization. *In*: Brockett RW, Millman RS, Sussmann HJ, Eds. *Differential Geometric Control Theory*. Birkhauser, Boston, USA, 181-191.

Chwa D (2011). Global tracking control of underactuated ships with input and velocity constraints using dynamic surface control method. *IEEE Transactions on Control Systems Technology*, **19**(6), 1357-1370.
DOI: 10.1109/TCST.2010.2090526

Do KD (2010a). Control of nonlinear systems with output tracking error constraints and its application to magnetic bearings. *International Journal of Control*, **83**(6), 1199-1216.
DOI: 10.1080/00207171003664828

Do KD (2010b). Practical control of underactuated ships. *Ocean Engineering*, **37**(13), 1111-1119.

DOI: 10.1016/j.oceaneng.2010.04.007

Do KD (2015). Global inverse optimal tracking control of underactuated omni-directional intelligent navigators (ODINs). *Journal of Marine Science and Application*, **14**(1), 1-13. DOI: 10.1007/s11804-015-1288-8

Do KD, Jiang ZP, Pan J (2002a). Underactuated ship global tracking under relaxed conditions. *IEEE Transactions on Automatic Control*, **47**(9), 1529-1536. DOI: 10.1109/TAC.2002.802755

Do KD, Jiang ZP, Pan J (2002b). Universal controllers for stabilization and tracking of underactuated ships. *Systems & Control Letters*, **47**(4), 299-317. DOI: 10.1016/S0167-6911(02)00214-1

Do KD, Jiang ZP, Pan J (2003). On global tracking control of a VTOL aircraft without velocity measurements. *IEEE Transactions on Automatic Control*, **48**(12), 2212-2217. DOI: 10.1109/TAC.2003.820148

Do KD, Jiang ZP, Pan J (2004). Robust adaptive path following of underactuated ships. *Automatica*, **40**(6), 929-944. DOI: 10.1016/j.automatica.2004.01.021

Do KD, Pan J (2004). State- and output-feedback robust path-following controllers for underactuated ships using Serret-Frenet frame. *Ocean Engineering*, **31**(5-6), 587-613. DOI: 10.1016/j.oceaneng.2003.08.006

Do KD, Pan J (2005). Global tracking control of underactuated ships with nonzero off-diagonal terms in their system matrices. *Automatica*, **41**(1), 87-95. DOI: 10.1016/j.automatica.2004.08.005

Do KD, Pan J (2006). Underactuated ships follow smooth paths with integral actions and without velocity measurements for feedback: Theory and experiments. *IEEE Transactions on Control Systems Technology*, **14**(2), 308-322. DOI: 10.1109/TCST.2005.863665

Encarnação P, Pascoal A, Arcak M (2000). Path following for autonomous marine craft. *Proceedings of the 5th IFAC Conference on Manoeuvring and Control of Marine Craft*, Girona, Spain, 117-122.

Fossen TI (2011). *Handbook of marine craft hydrodynamics and motion control*. John Wiley & Sons, West Sussex, England, 133-183.

Fredriksen E, Pettersen KY (2006). Global Kappa-exponential way-point maneuvering of ships: Theory and experiments. *Automatica*, **42**(4), 677-687. DOI: 10.1016/j.automatica.2005.12.020

Ghommam J, Mnif F, Benali A, Derbel N (2008). Nonsingular Serret-Frenet based path following control for an underactuated surface vessel. *Journal of Dynamic Systems, Measurement, and Control*, **131**(2), 021006. DOI: 10.1115/1.3023139

Godhavn JM, Fossen TI, Berge SP (1998). Non-linear and adaptive backstepping designs for tracking control of ships. *International Journal of Adaptive Control and Signal Processing*, **12**(8), 649-670. DOI: 10.1002/(SICI)1099-1115(199812)12:8<649::AID-ACS515>3.0.CO;2-P

Jiang ZP (2002). Global tracking control of underactuated ships by Lyapunov's direct method. *Automatica*, **38**(2), 301-309. DOI: 10.1016/S0005-1098(01)00199-6

Jiang ZP, Nijmeijer H (1999). A recursive technique for tracking control of nonholonomic systems in chained form. *IEEE Transactions on Automatic Control*, **44**(2), 265-279. DOI: 10.1109/9.746253

Khalil HK (2002). *Nonlinear systems*. Prentice Hall, Upper Saddle River, USA, 323-325.

Krstić M, Kanellakopoulos I, Kokotović PV (1995). *Nonlinear and adaptive control design*. Wiley, New York, USA.

Lapierre L, Jouvencel B (2008). Robust nonlinear path-following control of an AUV. *IEEE Journal of Oceanic Engineering*, **33**(2), 89-102. DOI: 10.1109/JOE.2008.923554

Lee TC, Jiang ZP (2004). New cascade approach for global κ-exponential tracking of underactuated ships. *IEEE Transactions on Automatic Control*, **49**(12), 2297-2303. DOI: 10.1109/TAC.2004.839632

Lefeber E, Pettersen KY, Nijmeijer H (2003). Tracking control of an underactuated ship. *IEEE Transactions on Control Systems Technology*, **11**(1), 52-61. DOI: 10.1109/TCST.2002.806465

Li A, Sun J, Oh S (2009). Design, analysis and experimental validation of a robust nonlinear path following controller for marine surface vessels. *Automatica*, **45**(7), 1649-1658. DOI: 10.1016/j.automatica.2009.03.010

Li JH, Lee PM, Jun BH, Lim YK (2008). Point-to-point navigation of underactuated ships. *Automatica*, **44**(12), 3201-3205. DOI: 10.1016/j.automatica.2008.08.003

Martin P, Devasia S, Paden B (1996). A different look at output tracking: control of a vtol aircraft. *Automatica*, **32**(1), 101-107. DOI: 10.1016/0005-1098(95)00099-2

Mazenc F, Pettersen K, Nijmeijer H (2002). Global uniform asymptotic stabilization of an underactuated surface vessel. *IEEE Transactions on Automatic Control*, **47**(10), 1759-1762. DOI: 10.1109/TAC.2002.803554

Moreira L, Fossen TI, Soares CG (2007). Path following control system for a tanker ship model. *Ocean Engineering*, **34**(14-15), 2074-2085. DOI: 10.1016/j.oceaneng.2007.02.005

Pettersen KY, Egeland O (1996). Exponential stabilization of an underactuated surface vessel. *Proceedings of 35th IEEE Conference on Decision and Control*, Kobe, Japan, 967-971.

Pettersen KY, Lefeber E (2001). Way-point tracking control of ships. *Proceedings of the 40th IEEE Conference on Decision and Control*, Orlando, USA, 940-945. DOI: 10.1109/.2001.980230

Pettersen KY, Nijmeijer H (2001). Underactuated ship tracking control: theory and experiments. *International Journal of Control*, **74**(14), 1435-1446. DOI: 10.1080/00207170110072039

Reyhanoglu M (1997). Exponential stabilization of an underactuated autonomous surface vessel. *Automatica*, **33**(12), 2249-2254. DOI: 10.1016/S0005-1098(97)00141-6

Skjetne R, Fossen TI (2001). Nonlinear maneuvering and control of ships. *Proceedings of OCEANS 2001 MTS/IEEE Conference and Exhibition*, Honolulu, USA, 1808-1815.